Biomed Microdevices (2009) 11:893–901
DOI 10.1007/s10544-009-9306-8

Localized surface plasmon resonance biosensor integrated with microfluidic chip

Chengjun Huang · Kristien Bonroy · Gunter Reekmans · Wim Laureyn · Katarina Verhaegen · Iwijn De Vlaminck · Liesbet Lagae · Gustaaf Borghs

Published online: 8 April 2009

Abstract A sensitive and low-cost microfluidic integrated biosensor is developed based on the localized surface plasmon resonance (LSPR) properties of gold nanoparticles, which allows label-free monitoring of biomolecular interactions in real-time. A novel quadrant detection scheme is introduced which continuously measures the change of the light transmitted through the nanoparticle-coated sensor surface. Using a green light emitting diode (LED) as a light source in combination with the quadrant detection scheme, a resolution of 10^{-4} in refractive index units (RIU) is determined. This performance is comparable to conventional LSPR-based biosensors. The biological sensing is demonstrated using an antigen/antibody (biotin/anti-biotin) system with an optimized gold nanoparticle film. The immobilization of biotin on a thiol-based self-assembled monolayer (SAM) and the subsequent affinity binding of anti-biotin are quantitatively detected by the microfluidic integrated biosensor and a detection limit of 270 ng/mL of anti-biotin was achieved. The microfluidic chip is capable of transporting a precise amount of biological samples to the detection areas to achieve highly sensitive and specific biosensing with decreased reaction time and less reagent consumption. The obtained results are compared with those measured by a surface plasmon resonance (SPR)-based Biacore system for the same binding event. This study demonstrates the feasibility of the integration of LSPR-based biosensing with microfluidic technologies, resulting in a low-cost and portable biosensor candidate compared to the larger and more expensive commercial instruments.

Keywords Localized surface plasmon resonance (LSPR) · Gold nanoparticle · Microfluidic · Biosensor

C. Huang (✉) · K. Bonroy · G. Reekmans · W. Laureyn · K. Verhaegen · I. De Vlaminck · L. Lagae · G. Borghs
Interuniversity Microelectronics Center (IMEC),
Kapeldreef 75,
B-3001 Leuven, Belgium
e-mail: chengjun.huang@yahoo.com

C. Huang · I. De Vlaminck
Department of Electrical Engineering (ESAT),
Katholieke Universiteit (KU) Leuven,
Kasteelpark Arenberg 10,
B-3001 Leuven, Belgium

1 Introduction

In recent years, microfluidic systems and lab-on-a-chip have received increasing interest because of their characteristic to obtain controlled mixing that can expedite chemical reactions, to reduce consumption of expensive materials and reagents, to reduce reaction time, to improve sensitivity, and to increase product yields (Deirdre and Mark 2002). Compact biosensors combined with microfluidics technologies have already been shown capable to provide faster and less expensive approaches to detect chemical and biomedical entities comparing with existing approaches that handle and detect biological samples in macro scale (Petra and Andreas 2006; Weigl et al. 2003). The high surface to volume ratio of the microfluidic device can enhance mass transport, resulting in shorter assay time and increased detection sensitivity (Erickson et al. 2008; Yuen et al. 2003).

Gold nanoparticles typically exhibit the localized surface plasmon resonance (LSPR) phenomenon, which is caused by the collective oscillations of the conductive electrons induced by visible light (Frederix et al. 2003; Willets and Van Duyne 2007). This LSPR property of the nanoparticles is sensitive to changes in surrounding

refractive index (RI). Previous researchers have studied different approaches to fabricate nanoparticles with various shapes and characteristics including chemical synthesis (Frederix et al. 2003), electron-beam lithography (Rechberger et al. 2003) and nanosphere lithography (Riboh et al. 2003) and have utilized LSPR effect for label-free detection of many biological molecules, such as glucose (Iwasaki et al. 2001), DNA (Hutter and Pileni 2003) and proteins (Fujiwara et al. 2006). A field of particular interest is the study of the antibody-antigen interaction (Haes and Van Duyne 2002; Lahav et al. 2004), where the LSPR biosensor can be used for sensitive sensing of a certain biomarker in a clinical setting, allowing the diagnosis of any disease using the associated antibody (Willets and Van Duyne 2007).

Although the optical properties of gold nanoparticles and their biosensing applications have been studied, even at a single-particle level (Kalkbrenner et al. 2004), there is very little research on the system integration of microfluidic technology and LSPR biosensing technology (Stuart et al. 2005). In most previous LSPR-based biosensing applications, batchwise and manual approaches were adopted for achieving sample loading, sample incubation and sample change. Such time-and labor-consuming operation drastically lowered the overall throughput and the assay speed, and neglected an important advantage of microfluidic systems in achieving high analytical speed. Recently, the conventional SPR biosensor system and its integration with microfluidics have been widely studied (De Leebeeck et al. 2007; Kim et al. 2007; Luo et al. 2008; Hoa et al. 2007). In these researches, a flat gold surface was most commonly used as a transducer and the Kretschmann configuration was usually involved with a prism for light-surface plasmon coupling at the gold surface. Based on this approach, some commercial devices are already available, such as Biacore system. However, these SPR-based systems usually required complicated optic system and were costly. In this study, we realized a functional gold nanoparticle biosensor with fully integrated microfluidics for LSPR-based biosensing. The proposed microfluidic integrated biosensor focused an incident light through a lens onto the biosensor surface that was divided into two areas, one for the reference and the other for sensing analyte. A novel, compact quadrant photo detection scheme was introduced and combined with a light emitting diode (LED) as a light source to form a transmission plasmon biosensing (TPB) platform and to continuously monitor the transmitted light through the nanoparticle-coated sensor surface. The performance and the sensitivity of the integrated system were tested with optimized gold nanoparticle films and its applicability for biosensing was demonstrated using an antigen/antibody (biotin/anti-biotin) model system.

2 Experiments and methods

2.1 Modeling of the LSPR response

A three-dimensional finite difference time-domain (FDTD) method (Lumerical, Vancouver, Canada) based on numerical solution of the Maxwell's equations was utilized to model the LSPR responses of the gold nanoparticles with different sizes from 14–43 nm. Experimental data of the frequency-dependent dielectric constants of Au, SiO_2 were fitted and used in the model. The frequency-dependent absorption cross-section in the gold nanoparticle film was extracted by monitoring the optical power flowing in and out of the volume with a total-field-scatter-field (TFSF) light source and perfectly matched layer (PML) type boundaries (Tanev et al. 2006).

2.2 Preparation and characterization of the nanoparticle-coated substrates

Gold nanoparticles with diameters ranging from 14–43 nm were prepared by sodium citrate reduction of hydrogen tetrachloroaurate ($HAuCl_4$) (Aldrich, Belgium) as described elsewhere (Frederix et al. 2003). Briefly, all glassware was cleaned using a freshly prepared mixture of HCl/HNO_3 (3: 1, v/v) and rinsed thoroughly in H_2O prior to use. In a typical synthesis of 43 nm gold nanoparticles, 6 mL of 1% (w/v) aqueous sodium citrate (Aldrich, Belgium) was added into a 750 mL boiling aqueous solution containing 0.01% (w/v) $HAuCl_4$. The suspension was boiled for an additional 5 min. The colloidal nanoparticles were then allowed to cool down to room temperature and stored at 4°C until needed. Smaller gold nanoparticles were prepared by increasing the molar ratio of sodium citrate to $HAuCl_4$ in the synthesis (Kim et al. 2006; Nath and Chilkoti 2004).

The gold nanoparticles were immobilized on substrates by using silane layer as a molecular glue [Nath and Chilkoti 2004; Frederix et al. 2003]. Prior to prepare the nanoparticle films, the quartz substrates (15 mm× 11.7 mm×1 mm) were cleaned in a piranha solution (H_2SO_4 : H_2O_2 = 3 : 1, v/v). Subsequently, the clean substrates were immersed for 3 hours in a solution containing 10% (v/v) 3-mercaptopropyltrimethoxy silane (Gelest Inc. USA) dissolved in a 95:5 ethanol/water (v/v) for silane deposition. Thereafter, the substrates were rinsed with ethanol, dried in a N_2 stream. Silane cross-linking was promoted in an oven for 10 min at 110°C. The substrates coated with gold nanoparticles were prepared by immersing the mercaptosilanized samples for 48 h in the gold nanoparticle suspension prepared as described above. Prior to use, the citrated capped gold nanoparticle film were thoroughly rinsed with water and dried in a N_2 stream.

Physical characterization of the nanoparticle films was performed using atomic force microscopy (AFM) (Dimension 3000/Nanoscope IV, Veeco) and transmission electron microscopy (TEM) (Philips CM12, Philips). The optical properties and the intrinsic sensitivity of the nanoparticle films were characterized using UV-vis spectrometer (Shimadzu UV-1601 PC).

For the biological experiments, the nanoparticle-coated substrates were further modified with a self-assembled monolayer (SAM) of thiols by 1 h incubation in 1 mM 16-mercapto hexadecanoic acid in ethanol and subsequently integrated with the microfluidic chips.

2.3 Integration of the microfluidic chips in combination with the nanoparticle-coated substrates

As the microfluidic integrated biosensor requires an optical read-out, a low absorption of the microfluidic material is indispensable between 400–750 nm, since this is the region where the nanoparticle film applied in this study absorbs light. The cyclic olefin copolymer (COC), among various polymer materials, was chosen because of its biocompatibility, microfabrication process compatibility, high optical transparency and low moisture absorption (Zou et al. 2007). In our work, the COC-based chip fabrication techniques have been developed and applied for high through-put and low-cost microfluidic chip fabrication by the Microfluidic Chip-shop Ltd. (Germany) and the Institut für Mikrotechnik Mainz Ltd. (IMM, Germany). Briefly, the microfluidic chip was replicated from a Ni mold with a 100 μm-thick plating microstructure over a 1 mm-thick COC substrate by injection molding. After drilling holes for fluidic interconnection at inlets and outlets, the chip was bonded thermally with a 188 μm-thick COC cover slide to form seal microchannels, as shown in Fig. 1. A double-sided sticky tape (thickness = 100 μm, 3 M Corp., USA) with two laser-cut detection windows was applied as a spacer to attach to the COC microfluidic chip on one side and to the nanoparticle-coated / blank substrate on the other side, forming a sandwich structure with two closed flow cells (L × W × H, 5 mm×5 mm×100 μm). Diamond-shape flow cells were designed in preventing air bubble formation. One of the flow cells (sample cell) has a nanoparticle-coated quartz substrate as a sensor surface and the other one is sealed with a blank quartz substrate without nanoparticles, serving as a reference cell. In this paper, we will refer to this assembled device as "microfluidic integrated biosensor".

2.4 Construction of the TPB readout

An optical TPB measurement setup was assembled, as shown schematically in Fig. 1. A LED (λ = 530 nm, λ_{FWHM} = 40 nm) (Linos Corp., USA) was used as a light source. The light beam was modulated with a chopper, collimated and focused with a lens, distributing equally on both the sample and the reference cells of the microfluidic integrated biosensor. The light transmitted through the two cells was detected with a quadrant photodetector with four cells of A, B, C, D (New focus Corp., USA) and was converted to three voltage output signals: the differential signals of X (= (B + C)–(A + D)) and Y (= (A + B)–(C + D)) and the SUM signal (= A + B + C + D) (Fig. 1). Since X and Y have similar definitions, only X and SUM signals were used in the described experiment and were accumulated with a lock-in amplifier (SR830, Stanford Research Systems, USA). Prior to each measurement, the system was calibrated to balance the left component (A + D) (sample cell) and the right component (B + C) (reference cell). The microfluidic integrated biosensor was inserted into the center of the incident beam by a home-made holder. The fluidic flows were driven by a syringe pump (Harvard Apparatus, USA) and passed through the two flow cells. A custom-coded program was used to record and to plot the real-time response of the quadrant photodetector. Upon the binding of analytes to the sensor surface, the transmission light shifted accordingly. The difference of transmitted light intensities between the light beam passing through the sample cell and that passing through the reference cell was called the transmission signal. This transmission signal was obtained by computing the signal of X from the output of the quadrant photodetector and was plotted as a function of time. The SUM signal (=A+B + C+D) was provided as a mean of normalization to ensure all measurements were performed under the same illumination condition.

2.5 Biological testing

For the biosensing measurements, both flow cells, the sample and reference, were flushed with a running buffer of Hepes Buffered Saline (HBS) for 10 min at 50 μL/min until a stable baseline was obtained. Subsequently, a 1:1 (v/v) mixture of 0.4 M EDC (3-3(dimethylaminopropyl)-1-ethylcarbodiimide) and 0.1 M NHS (N-hydroxysulfo-succinimide sodium salt) was injected at 20 μL/min into both flow cells for 10 min, followed by 6 min injection of 5 mM maleate buffer (pH = 6.0) at 20 μL/min. The biotin molecules were immobilized on the gold nanoparticle surface by 16 min incubation with 500 μg/mL NH_2-biotin (Pierce Inc., Italy) in maleate buffer at 20 μL/min, followed by 4 min incubation of 1 M triethyleneglycol monoamine (50 μL/min) to block the surface and to reduce the non-specific binding. Afterwards, both flow cells were flushed with HBS for 15 min at 50 μL/min.

To detect the antigen-antibody interaction, the biotin immobilized sensor surfaces were further incubated with various concentrations of goat anti-biotin solution (Pierce Inc., Italy) dissolved in HBS at 20 μL/min for 20 min,

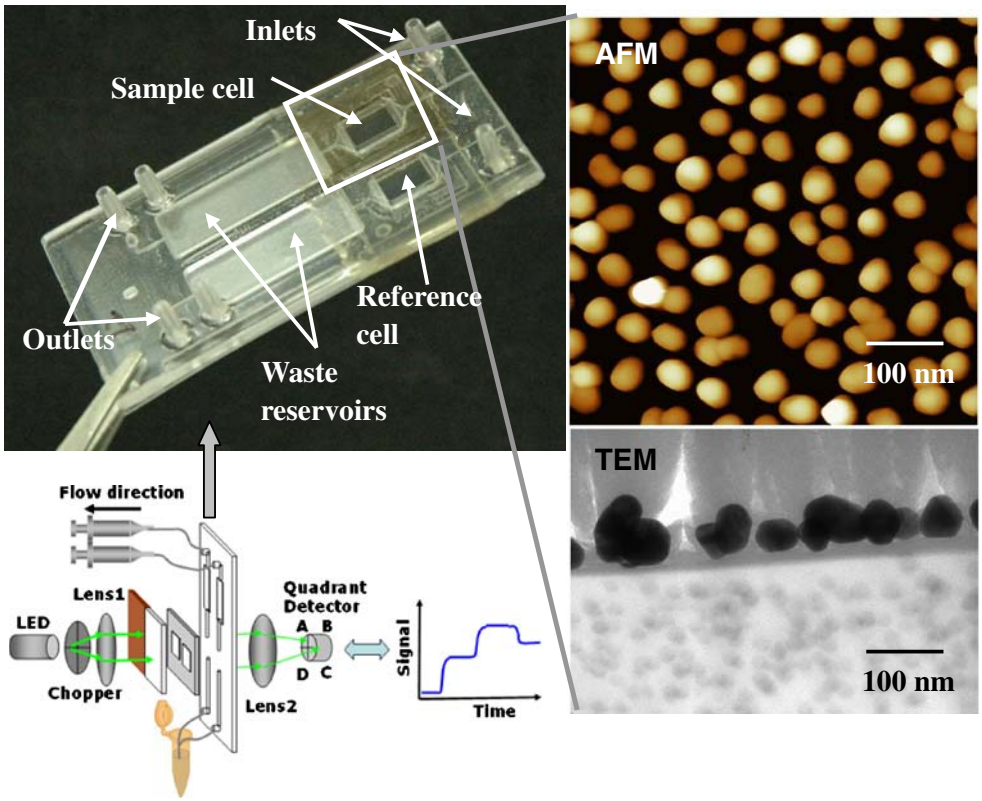

Fig. 1 (a) Schematic the TPB readout platform and photograph of the microfluidic integrated LSPR biosensor. The inset shows the AFM and TEM images of the gold nanoparticle film with nanoparticle diameter = 43 nm. Scale bar = 100 nm

followed by 10 min HBS flush. The whole procedure was monitored by the developed TPB platform with a sampling frequency of 0.5 Hz. All the measurements were performed at room temperature unless otherwise specified. All the buffers were degassed and filtered before use.

As confirmation experiments, similar biotin/anti-biotin recognition experiments were performed by a Biacore 2000® system (Biacore AB, Uppsala, Sweden) using standard protocols in combination with flat gold samples (Bonroy et al. 2006). Briefly, the clean gold substrate was first modified with a SAM of thiols and then mounted on the Biacore chip holder. After docking the chip in the system, different solutions, mixture of EDC/NHS, biotin, triethyleneglycol monoamine were injected sequentially into the Biacore system. Anti-biotin solutions with different concentrations in HBS were injected over the biotin coated surface. The surface was re-generated by two pulses of 10 mM glycine-HCl (pH = 2.2) between each anti-biotin injection. The SPR response shift in resonance units (RU) upon biomolecular binding were evaluated.

3 Results and discussion

3.1 Simulated LSPR spectra of gold nanoparticles

Figure 2(a) shows the spectra of absorption cross-section of the gold nanoparticles with diameters ranging 14–43 nm and with surrounding RI of 1.333, which exhibit clear resonance behaviors. As the increase of the diameter of the nanoparticle, the maximum absorption increases and the peak position red-shifts. In Fig. 2(b), the electrical field distributions of a typical gold nanoparticle films (Au sphere_43 nm) are plotted for an off-resonant excitation wavelength (750 nm) and for an on-resonance excitation wavelength

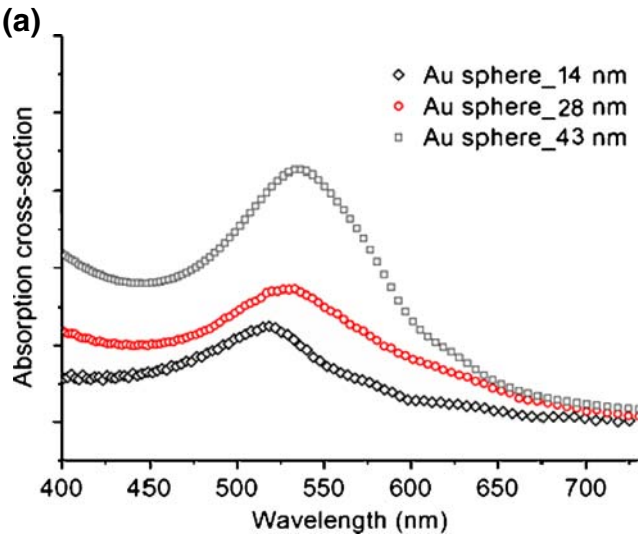

Fig. 2 (a) Simulated spectra of absorption cross-section of gold nanoparticles with different sizes **(b)** Electric field distribution of a typical gold nanoparticle film with nanoparticle diameter = 43 nm at different excitation wavelengths

Fig. 2 (continued)

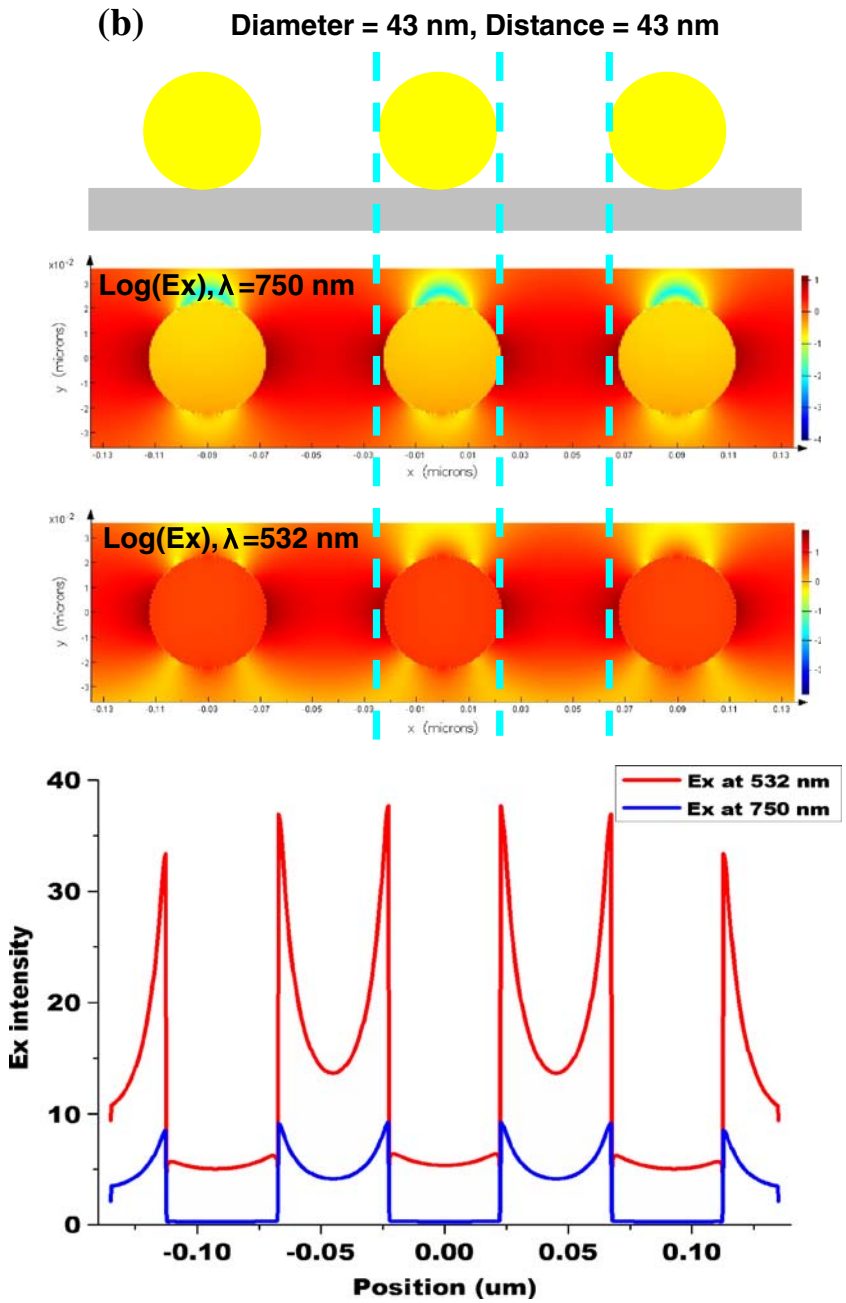

(532 nm). In the latter case, the electrical field is strongly amplified both in the nanoparticles and in the local environments of the nanoparticles. The plasmon-enhanced electrical field leads to enhanced light absorption, thus giving a maximum absorption at 532 nm in the absorption spectrum (Fig. 2(a), spectrum of Au sphere_43 nm).

3.2 Characterization of the nanoparticle films

As the size, the morphology, and the surrounding RI of the gold nanoparticles significantly affect the sensitivity of the LSPR-based biosensor (Nath and Chilkoti 2004), it is important to select the most sensitive nanoparticle film for our biosensor application. We synthesized various gold nanoparticles with different sizes and deposited them on the quartz substrates using a mercaptosilane layer as molecular glue. Their sensitivities to the changes of surrounding RI were evaluated experimentally. The different nanoparticle films were mounted in a modified cuvette (Frederix et al. 2003) and their spectra were measured in water (n = 1.333) and in different glycerol solutions with different RI by the UV-vis spectrometer. Figure 3 shows the calibration between the maximum absorbance and the surrounding RI for the nanoparticle films of 14 nm, 28 nm and 43 nm. For

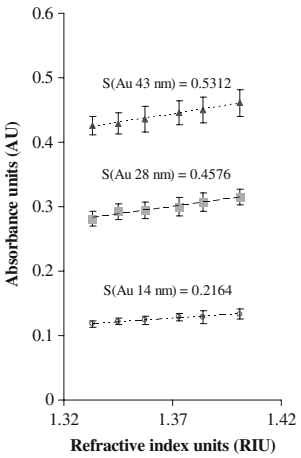

Fig. 3 Plots of the maximum absorbance (measured by UV-vis spectrometer) of the different nanoparticle films as a function of surrounding RI

all of these three nanoparticle films, the maximum absorbance exhibits a linear relationship as a function of the surrounding RI caused by the glycerol solutions (Mitsui et al. 2004; Nanduri et al. 2007). The slope (S) of the linear curves can serve as a measure for the intrinsic sensitivity of the nanoparticle film. The film with nanoparticle diameter = 43 nm exhibits a maximum sensitivity to the changes of the surrounding RI, which is consistent with the reported results (Nath and Chilkoti 2004). Consequently, the 43 nm nanoparticle film was chosen for our application.

The nanoparticles size, distribution and density on the quartz substrates were verified by AFM and TEM. The measured nanoparticles sizes were 14±3 nm, 28±4 nm and 43±7 nm, respectively. The AFM and TEM images of the 43 nm nanoparticle film (Fig. 1) show a monolayer distribution of gold nanoparticles coated onto the quartz substrate. Both AFM and TEM images show that the nanoparticles are not touching but they are isolated with an interval of the same magnitude as the nanoparticle's diameter. To evaluate the nanoparticle densities, we took different AFM images which were captured randomly from different regions of the nanoparticle film and different samples. We counted the immobilized particles on the AFM analyzed region (1 μm × 1 μm) and determined the nanoparticle film (43 nm) selected for our application had a particle density of 105±4 particles/μm^2.

3.3 Characterization of the microfluidic integrated biosensor

To optimize the wavelength of the light source and to test the influence of the microfluidics on the intrinsic sensitivity of the nanoparticle film (Au 43 nm), the UV-vis spectrometer was used for the optical characterization of the microfluidic integrated biosensor. Figure 4 shows the absorbance spectra of the biosensor when injecting different glycerol solutions at 50 μL/min sequentially. By changing the surrounding RI of the nanoparticles, a red-shift of the peak position and an increase of the maximum absorbance occur. These variations in microfluidic condition are in good agreement with the previously reported results measured in cuvette statically, without the microfluidic chip (Ye et al. 2008). Furthermore, if we make a vertical line along 530 nm wavelength, plot the absorbance intensities of the intersections of the spectra and the 530 nm line as a function of surrounding RI, a good linear relationship between them was determined as shown in Fig. 4 (the inset). This result indicates the feasibility of a single-wavelength measurement of the LSPR effect at the off-peak wavelength, such as 530 nm (Nath and Chilkoti 2004). Meanwhile, our results also show that the 530 nm wavelength of the light source is the best choice for performing biosensing with our selected nanoparticle film. Therefore a compact LED (λ=530 nm) was chosen for our TPB platform, which can provide an intensity-tunable light beam. Moreover, this LED light source can also be easily replaced with a new one with different wavelength if necessary. A single-wavelength measurement in our experiment shows more experimental flexibility and is preferable for kinetic measurements of receptor-analyte binding (Nath and Chilkoti 2004) and is more suited for parallelization.

Once the microfluidic integrated biosensor was tested in the commercial UV-vis spectrometer, we transferred it to our home-made TPB readout platform. Figure 5 shows the real-time transmission response of the biosensor measured by the TPB platform when injection different glycerol solutions at 50 μL/min sequentially. A stepwise increase in transmission response is observed as the surrounding RI increase, which means the difference between the transmitted light beams passing through the nanoparticle-coated substrate (in sample cell) and blank substrate (in reference cell) also increases due to the LSPR effect. The shift of the transmission response exhibits a very good linear relation-

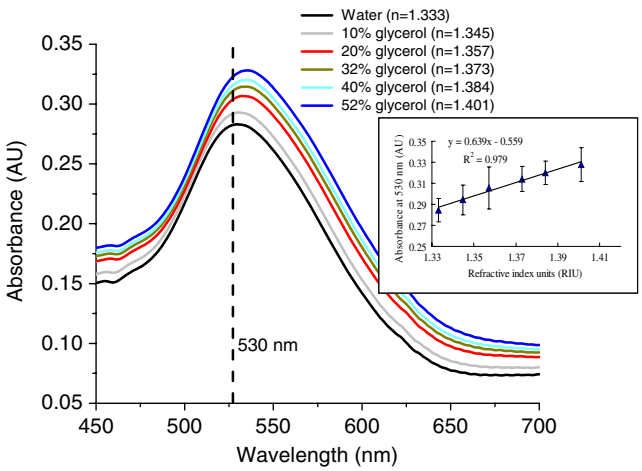

Fig. 4 UV-vis spectra of the microfluidic integrated biosensor when injecting different glycerol solutions. The inset is the plot of the absorbance at 530 nm as a function of the RI

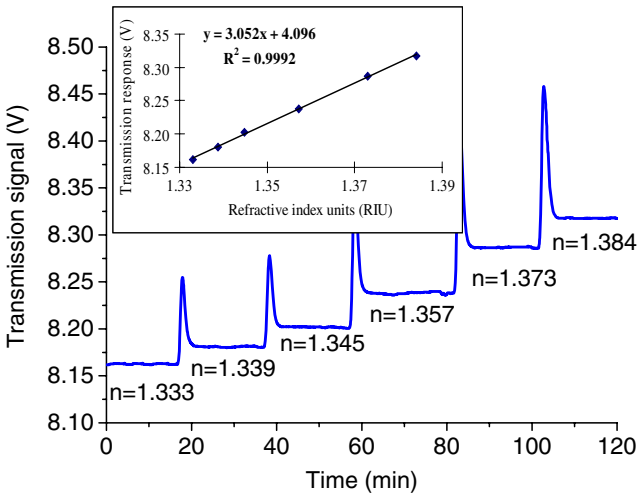

Fig. 5 Real-time transmission response of the microfluidic integrated biosensor when injecting different glycerol solutions. The inset is the plot of the transmission response as a function of the surrounding RI. The error bar is not visible in the plot due to the small value

ship, which agrees well with the UV-vis absorbance spectra. Because the signals from the two areas of the biosensor were produced and detected with the same LED light source, optics, and photodetector, all common noises, such as light intensity fluctuation and thermal drift are subtracted out, thus providing a simple and accurate approach to measure the shift of the transmitted light. A refractive index resolution of 10^{-4} RIU was determined according to the calibration curve (Fig. 5, inset), which was comparable to conventional LSPR biosensors (Hoa et al. 2007). We notice that there are sharp changes in the transmission response that coincide with the moments where different solutions are introduced into the flow cells. These sharp changes correspond to the inhomogeneous mixing of the fresh injecting solution (Zhang et al. 2003) and disappear after a uniformed mixing is achieved, usually within 2 min after each injection. The deviation of the signals is less than 0.2% when a stable measurement signal is achieved, which confirms the stability of our microfluidic integrated biosensor. Since the sharp changes due to inhomogeneous mixing of samples have no influence on signals and can be easily eliminated by subsequent data processing, they will be ignored in following measurements for clarity.

3.4 Detection of biotin/anti-biotin affinity binding on the TPB platform

Figure 6(a) shows a typical real-time transmission response of the microfluidic integrated biosensor corresponding to the biomolecular interaction recorded by the TPB platform. An initial signal of 7.021 V (Curve 1 in Fig. 6(a)) was recorded when both of the sample and reference cells were flushed with the running buffer of HBS. Afterwards, an EDC/NHS linker was used to covalently attach biotin to the carboxylate group on the sensor surface. The binding of biotin resulted in an increase of 0.045 V to 7.066 V (Curve 2 in Fig. 6(a)). In a next step, the recognition of 30 μg/mL anti-biotin on the biotin functionalized sensor resulted in a further signal increase of 0.579 V, giving rise to a final transmission response of 7.645 V (Curve 3 in Fig. 6(a)). Finally, by introduction of 10 mM Glycine-HCl solution (pH = 2.2) for 5 min, the transmission response of 7.645 V after the anti-biotin recognition went back to the original level of 7.067 V (Curve 4 in Fig. 6(a)) as that of before the

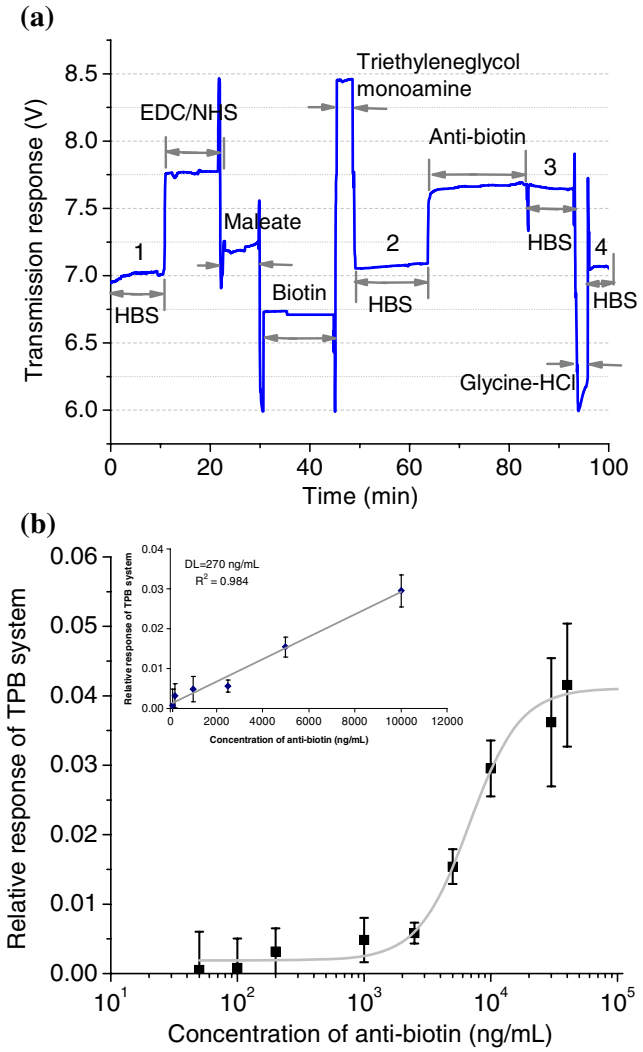

Fig. 6 **(a)** Typical real-time transmission response of the microfluidic integrated biosensor for biotin/anti-biotin assay. The numbers indicate the four different experimental procedures: (1) measurement in HBS before the biotin immobilization; (2) measurement in HBS after the biotin immobilization; (3) measurement in HBS after the anti-biotin recognition; (4) measurement in HBS after the dissociation of anti-biotin. **(b)** Plot of the relative changes of transmission response as a function of anti-biotin concentration. The error bars represented the standard deviation with n ≥ 3. The inset shows the linear fitting of the dose-response curve in the linear response range (100 ng/mL to 10 μg/mL anti-biotin) for detection limit calculation

recognition. This indicates the lowering of the surrounding RI of the gold nanoparticles, which is attributable to the dissociation of anti-biotin from biotin. The obtained results also bring a possibility to regenerate the sensor surface and to re-use the device.

The concentration dependence of anti-biotin recognition was investigated from 50 ng/mL to 40 μg/mL (Fig. 6(b)). The relative change of the transmission response before and after the anti-biotin recognition with various concentrations, $(T_{after}-T_{before})/T_{before}$, were calculated and were plotted using a dose-response curve fit. To estimate the sensitivity and detection limit (DL), the data were collected by measuring the signal changes caused by anti-biotin with various concentrations on different devices from the same batch. The curve was partially fitted linearly and the slope was taken as a measure for the sensitivity and the error bars represented the standard deviation on at least three independent measurements ($n \geq 3$). The DL in ng/mL was calculated using the method described elsewhere (Peeters et al. 2008; De Palma et al. 2007; Riboh et al. 2003) and a DL of 270 ng/mL anti-biotin was achieved. Further improvements on DL can be expected from optimization of the nanoparticle film (Larsson et al. 2007) and the microfluidic system (Sheehan and Whiteman 2005).

3.5 Comparison with UV-vis measurement and SPR-based measurement

With the development of a new sensor platform, it is necessary to compare it with relevant systems which are already commercially available. In this study, we compared our TPB platform and its microfluidic integrated biosensor with the widely used UV-vis spectrometer, as well as the Biacore system. If one compares the binding events happening under different conditions, i.e. fluidic incubation in this study and static incubation in previous research (Endo et al. 2005; Fujiwara et al. 2006; Haes and Van Duyne 2002; Riboh et al. 2003), one can find that our microfluidic integrated biosensor can greatly reduce the reaction time and reagent consumption due to its small volume and high surface area to volume ratio (Yuen et al. 2003). For instance, according to Riboh's report (Riboh et al. 2003), it took 3 h for the incubation of anti-biotin recognition in static condition, which we could decrease to about 20 min for a similar biotin/anti-biotin assay in a microfluidic chip. On top of that our microfluidic chip also allowed the transport of the precise amount of samples to the detection area and therefore the reagent consumption could be decreased from several milliliters in conventional measurements (Endo et al. 2005; Fujiwara et al. 2006; Haes and Van Duyne 2002; Riboh et al. 2003) to less than half a milliliter in this study. The obtained results confirm the need for an integrated microfluidic system (Yuen et al. 2003) which is of particular importance for point-of-care diagnostic applications.

Moreover, our TPB platform in combination with the microfluidic integrated biosensor provided a real-time monitor of the biomolecular interaction rather than a single result-measurement. For instance, for the anti-biotin incubation curve as shown in Fig. 6(a), during the first 10 min, the signal increases as a function of the incubation time, which indicates more and more anti-biotin molecules are bound on the sensor surface. However, ~ 10 min later, the signal saturates at a certain level. This dynamic curve is useful for the investigation of the kinetic biomolecular interactions and also indicates that the incubation time can probably be further decreased.

To form an idea on the amount of anti-biotin binding on the surface at different concentrations in an alternative approach and to evaluate if the obtained transmission signal of our TPB measurement follow the same trend as the signal measured by a well-known microfluidic integrated SPR system (i.e. Biacore system), similar biotin/anti-biotin experiments were performed with a Biacore system. Figure 7 shows a typical SPR response curve with a similar shape as the transmission response obtained from the TPB platform (Fig. 6(a) and Fig. 7). The cross comparison of the transmission response shift (measured by our TPB system) caused by anti-biotin binding for the five different anti-biotin concentrations ranging 200 ng/mL to 30 μg/mL (y-axis) versus the SPR response shift (measured by the Biacore system) for the corresponding concentrations (x-axis) yields a correlation coefficient of 0.975, indicating that the results of the TPB measurements by our system agree quantitatively with those measured by the commercial Biacore system. The reliability of our TPB system, in combination with the advantages of the ease of chemical fabrication of the sensor, its small size,

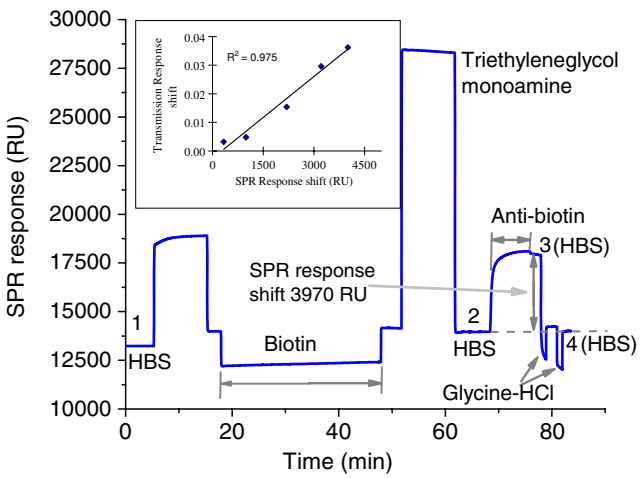

Fig. 7 Typical SPR sensorgram of the Biacore system for biotin/anti-biotin assay. The inset is the correlation between TPB system and the Biacore system

no temperature control requirement (Stuart et al. 2005), the very low system and reagent costs make the sensor especially suitable for field applications.

4 Conclusions

In this research, we have successfully demonstrated an LSPR biosensor integrated with a microfluidic chip, as well as a compact readout platform for real-time TPB measurements. Our approach provided a direct way to couple the sensitive, label-free LSPR biosensors with a compact microfluidic platform, thus taking advantages from both technologies. It brought a promising example of plasmofluidics (Liu et al. 2006; Mao et al. 2007), an emerging field that fuses plasmonics and microfluidics and enable the development of both surface plasmon-based "lab-on-a-chip" and fluid-based active plasmonics.

Acknowledgements The research described in this paper is performed in the frame of the smartHEALTH Integrated Project, which is partially funded by the European Commission under contract No. 016817. The authors would also like to thank the Microfluidic Chip-shop Ltd. (Germany) and the Institut für Mikrotechnik Mainz Ltd. (IMM, Germany) for their help and for the fabrication of the microfluidic chip.

References

K. Bonroy, F. Frederix, G. Reekmans, E. Dewolf, R. De Palma, G. Borghs, P. Declerck, B. Goddeeris, J. Immunol. Methods **312**, 167–181 (2006). doi:10.1016/j.jim.2006.03.007

A. De Leebeeck, L.K. Kumar, V. de Lange, D. Sinton, R. Gordon, A.G. Brolo, Anal. Chem **79**, 4094–4100 (2007). doi:10.1021/ac070001a

R.M. Deirdre, R.H. Mark, Science **297**, 1197–1198 (2002). doi:10.1126/science.297.5584.1197

R. De Palma, G. Reekmans, W. Laureyn, G. Borghs, G. Maes, Anal. Chem **79**, 7540–7548 (2007). doi:10.1021/ac0713407

T. Endo, S. Yamamura, N. Nagatani, Y. Morita, Y. Takamura, E. Tamiya, Sci. Technol. Adv. Mater **6**, 491–500 (2005). doi:10.1016/j.stam.2005.03.019

D. Erickson, S. Mandal, A.H.J. Yang, B. Cordovez, Microfluid. Nanofluid **4**, 33–52 (2008). doi:10.1007/s10404-007-0198-8

F. Frederix, J.M. Friedt, K.H. Choi, W. Laureyn, A. Campitelli, D. Mondelaers, G. Maes, G. Borghs, Anal. Chem **75**, 6894–6900 (2003). doi:10.1021/ac0346609

K. Fujiwara, H. Watarai, H. Itoh, E. Nakahama, N. Ogawa, Anal. Bioanal. Chem **386**, 639–644 (2006). doi:10.1007/s00216-006-0559-2

A.J. Haes, R.P. Van Duyne, J. Am. Chem. Soc **124**, 10596–10604 (2002). doi:10.1021/ja020393x

X.D. Hoa, A.G. Kirk, M. Tabrizian, Biosens. Bioelectron **23**, 151–160 (2007). doi:10.1016/j.bios.2007.07.001

E. Hutter, M.P. Pileni, J. Phys. Chem. B **107**, 6497–6499 (2003). doi:10.1021/jp0342834

Y. Iwasaki, T. Horiuchi, O. Niwa, Anal. Chem **73**, 1595–1598 (2001). doi:10.1021/ac0012851

T. Kalkbrenner, U. Hakanson, V. Sandoghdar, Nano Lett **4**, 2309–2314 (2004). doi:10.1021/nl048694n

C.K. Kim, R.R. Kalluru, J.P. Singh, A. Fortner, J. Griffin, G.K. Darbha, P.C. Ray, Nanotechnology **17**, 3085–3093 (2006). doi:10.1088/0957-4484/17/13/001

S.J. Kim, K.V. Gobi, H. Iwasaka, H. Tanaka, N. Miura, Biosens. Bioelectron **23**, 701–707 (2007). doi:10.1016/j.bios.2007.08.010

M. Lahav, A. Vaskevich, I. Rubinstein, Langmuir **20**, 7365–7367 (2004). doi:10.1021/la0489054

E.M. Larsson, J. Alegret, M. Käll, D.S. Sutherland, Nano Lett **7**, 1256–1263 (2007). doi:10.1021/nl0701612

G.L. Liu, J. Kim, Y. Lu, P.L. Lee, Nat. Mater **5**, 27–32 (2006). doi:10.1038/nmat1528

Y.Q. Luo, Y. Fang, R.N. Zare, Lab Chip **8**, 694–700 (2008). doi:10.1039/b800606g

X.L. Mao, J.R. Waldeisen, B.K. Juluri, T.J. Huang, Lab Chip **7**, 1303–1308 (2007). doi:10.1039/b708863a

K. Mitsui, Y. Handa, K. Kajikawa, Appl. Phys. Lett **85**, 4231–4233 (2004). doi:10.1063/1.1812583

V. Nanduri, A.K. Bhunia, S.I. Tu, G.C. Paoli, J.D. Brewster, Biosens. Bioelectron **23**, 248–252 (2007). doi:10.1016/j.bios.2007.04.007

N. Nath, A. Chilkoti, Anal. Chem **76**, 5370–5378 (2004). doi:10.1021/ac049741z

S. Peeters, T. Stakenborg, G. Reekmans, W. Laureyn, L. Lagae, A. Van Aerschot, M. Van Ranst, Biosens. Bioelectron **24**, 72–77 (2008). doi:10.1016/j.bios.2008.03.012

S.D. Petra, M. Andreas, Nat. Rev. Drug Discov **5**, 210–218 (2006). doi:10.1038/nrd1985

W. Rechberger, A. Hohenau, A. Leitner, J.R. Krenn, B. Lamprecht, F. R. Aussenegg, Opt. Commun **220**, 137–141 (2003). doi:10.1016/S0030-4018(03)01357-9

J.C. Riboh, A.J. Haes, A.D. McLFarland, C.R. Yonzon, R.P. Van Duyne, J. Phys. Chem. B **107**, 1772–1780 (2003). doi:10.1021/jp022130v

P.E. Sheehan, L.J. Whiteman, Nano Lett **5**, 803–807 (2005). doi:10.1021/nl050298x

D.A. Stuart, A.J. Haes, C.R. Yonzon, E.M. Hicks, R.P. Van Duyne, I. E.E. Proc. Nanobiotechnol **152**, 13–32 (2005). doi:10.1049/ip-nbt:20045012

S. Tanev, V.V. Tuchin, P. Paddon, Laser Phys. Lett **3**, 594–598 (2006). doi:10.1002/lapl.200610052

B.H. Weigl, R.L. Bardell, C.R. Cabrera, Adv. Drug Res **55**, 349–377 (2003). doi:10.1016/S0169-409X(02)00223-5

K.A. Willets, R.P. Van Duyne, Annu. Rev. Phys. Chem **58**, 267–297 (2007). doi:10.1146/annurev.physchem.58.032806.104607

J. Ye, K. Bonroy, D. Nelis, F. Frederix, J. D'Haen, G. Maes, G. Borghs, Colloids Surf. A Physicochem. Eng. Asp **321**, 313–317 (2008). doi:10.1016/j.colsurfa.2008.01.028

P.K. Yuen, G.S. Li, Y.J. Bao, U.R. Muller, Lab Chip **3**, 46–50 (2003). doi:10.1039/b210274a

H.Q. Zhang, S. Boussaad, N.J. Tao, Rev. Sci. Instrum. **74**, 150–153 (2003). doi:10.1063/1.1523649

Z.W. Zou, J.H. Kai, M.J. Rust, J. Han, C.H. Ahn, Sens. Actua **A 136**, 518–526 (2007). doi:10.1016/j.sna.2006.12.006